Hybrid quantum dot–superconducting systems: Josephson current and Kondo effect in the narrow-band limit

R. Allub
Centro Atómico Bariloche, C.P. 8400, San Carlos de Bariloche, Río Negro, Argentina

C. R. Proetto
Centro Atómico Bariloche and Instituto Balseiro, C.P. 8400, San Carlos de Bariloche, Río Negro, Argentina
(Received 23 July 2014; revised manuscript received 15 December 2014; published 30 January 2015)

The case of a quantum dot connected to two superconducting leads is studied by using the narrow-band limit to describe the superconducting degrees of freedom. The model provides a simple theoretical framework, almost analytical, to analyze the interplay between the Kondo effect, superconductivity, and finite temperature. In the quantum dot Kondo regime, the model is completely characterized by the ratio Δ/J, with Δ the superconducting gap and J an effective antiferromagnetic exchange coupling between the dot and the leads. The model allows us to calculate, at any temperature T, the equilibrium Josephson current through the dot in a very straightforward way as a function of Δ/J. The behavior of the current allows us to distinguish the four types of hybrid junctions: 0, 0′, π', and π. The presence of the 0- and 0′-junction configurations are intrinsically linked to the Kondo effect in the quantum dot, while the π- and π'-junction configurations are driven by the superconductivity in the leads. The Josephson critical current has a non-monotonic behavior with temperature, that may be used for the experimental characterization of the fundamental $0-\pi$ transition. The model allows us to obtain easily a phase diagram Δ/J vs temperature, from where we can obtain an overall picture on the stability of the different types of junctions. From the explicit analytical expressions for the ground-state, low-energy excitations, free energy, and Josephson current, it is easy to understand the physical nature of the main features of the critical current and the phase diagram. The results, obtained with a minimum of numerical effort, are in a good qualitative agreement with more demanding calculational approaches aimed to solve the full model.

DOI: 10.1103/PhysRevB.91.045442 PACS number(s): 74.50.+r, 72.15.Qm, 75.20.Hr

I. INTRODUCTION

The interplay between the Kondo physics and the Josephson current through a quantum dot (QD) connected to superconducting reservoirs has triggered an intense interest on this topic in recent years [1]. Before that, early and pioneering experiments in semiconductor quantum dots (QD) coupled to normal (no-superconductor) metallic leads already attracted the attention of the physics community since they provide a unique tool to recreate the electronic and magnetic properties of many different isolated atomic systems immersed in a metallic matrix [2]. Among the more attractive features of the QD's systems is the possibility of changing in a controllable way the parameters characterizing the dots (i.e., the discrete energy levels of the single-electron states, the total number of electrons, the Coulomb repulsion among the localized dot electrons, the hybridization with the leads, etc.). Due to this fact, it is possible to study with unprecedented detail many different physical phenomena such as the Coulomb blockade [3], the Kondo effect [4,5], and different electronic transport properties [3,6].

On the other side, the traditional Josephson effect involves two macroscopic superconductors with a weak link, usually an insulating barrier, between them. Each superconductor is characterized by an order parameter or phase φ, and if it happens that there is a difference of phase $\Delta\varphi$ between the two superconductors, a dissipationless supercurrent may flow through the weak link, $I(\Delta\varphi) = J_c \sin(\Delta\varphi)$, with J_c being the junction critical current, which depends both on the size of the superconducting gap, and on the transmission amplitude of the weak link [7]. This sinusoidal dependence of the Josephson current with the phase difference $\Delta\varphi$ is the landmark of the Josephson effect, and is widely used in standard superconducting devices such as the SQUIDs (superconducting quantum interference devices) [8] and superconducting quantum bits or qubits [9].

The possibility of replacing the normal metallic leads by superconducting ones added a new twist to the QD-atomic systems analogy commented above: in 1977 it was predicted that magnetic impurities in the insulating layer could lead to a reversal of the Josephson current in a Josephson junction, $I(\Delta\varphi) = -J_c \sin(\Delta\varphi)$ [10]. This situation was characterized as the "π-junction" behavior [11]. And since the quantum dot behaves in many ways like atomic magnetic impurities, the question arises quite naturally: will it be possible to have π-junction behavior for a quantum dot connected to two superconductor leads? And the answer is yes, both from the experimental and the theoretical point of view. On the experimental side, researchers have explored the consequences of replacing the thin insulating barrier between the two superconductors by a nanoscale superconducting or normal metal bridge [12], a carbon nanotube [13,14], or a semiconductor quantum dot [15], as commented above. This latter case is the one to which the present work is devoted. The interplay between Kondo screening and superconductivity has been also recently studied with unprecedented experimental detail in these hybrid systems [16]. The coupling of two superconductors through a ferromagnetic link has been also experimentally realized [17]. An exciting new research avenue has been open since the observation of signatures of Majorana fermions in hybrid superconductor-semiconductor nanowire devices [18].

On the theoretical side, the "standard" model towards an understanding of this very interesting problem has been the Anderson impurity model (representing the dot) connected

to Bardeen-Cooper-Schrieffer (BCS) superconducting leads. A complete and update review on these hybrid systems may be found in Ref. [19]. In spite of the simplifications leading to the setting of the model, its solution still is a formidable task, due to the simultaneous presence of strong correlations inside the dot, superconductivity in the leads, and intrinsic temperature effects. As a consequence, different theoretical schemes have been used to attack the problem, including quantum Monte Carlo (QMC) calculations [20], numerical renormalization group (NRG) approaches [21,22], the noncrossing approximation [23,24], and the functional renormalization group (FRG) [22]. In order to obtain the model results, most of these methods require large numerical effort. Among other interesting theoretical schemes applied recently to these hybrid systems we can cite also the expansion in powers of the inverse of the superconducting gap size [25] and the continuous time quantum Monte Carlo approach [26]. A generalized Schrieffer-Wolff transformation has been also used to simplify the analysis of the coupling between the QD and the superconducting leads of the standard model [27]. The aim of this paper is to present a much simpler approach which qualitative describes the basic physics involved in the interplay between the Kondo effect and the Josephson current, at *zero and finite temperature*.

In the following section we introduce the model Hamiltonian and set up the narrow-band limit to this problem. In Sec. III, we obtain and analyze the free energy, the equilibrium Josephson current, and provide a global phase diagram of the model. Finally, Sec. IV consists of the conclusions.

II. MODEL

The standard model to describe the physics of a quantum dot coupled to two superconducting leads (L and R) can be written as

$$H = H_s + H_d + H_t, \tag{1}$$

where H_s corresponds to the superconducting leads, H_d describes the QD by the Anderson impurity model, and H_t is the tunneling Hamiltonian between the QD and the leads. The leads are considered to be s-wave superconductors and described by a BCS-like Hamiltonian, as follows:

$$H_s = \sum_{k,p,\sigma} \varepsilon_k c^\dagger_{k,p,\sigma} c_{k,p,\sigma} - \sum_{k,p} \Delta_s [e^{i\varphi_p} c^\dagger_{k,p,\uparrow} c^\dagger_{k,p,\downarrow} + \text{H.c.}], \tag{2}$$

where ε_k is the energy of the state k in the leads, and $c^\dagger_{k,p,\sigma}$ ($c_{k,p,\sigma}$) creates (annihilates) an electron with spin σ, in the lead p (L or R) and momentum k. Δ_s is the superconducting gap and φ_p is the phase of the superconducting order parameter in the p lead. The two leads are assumed to be identical except for the phases φ_L and φ_R. Without loss of generality we take $\varphi_L = -\varphi_R = \varphi/2$, which implies that $\varphi_L + \varphi_R = 0$, and $\Delta\varphi = \varphi_L - \varphi_R = \varphi$.

The QD Hamiltonian is given by

$$H_d = \sum_\sigma \varepsilon_d \, d^\dagger_\sigma d_\sigma + U \, d^\dagger_\uparrow d_\uparrow d^\dagger_\downarrow d_\downarrow \, , \tag{3}$$

where $d^\dagger_\sigma$ (d_σ) creates (annihilates) an electron with spin σ on the QD with energy ε_d and the interaction $U(>0)$ is of the order of the charging energy $e^2/2C$, with C the capacitance of the QD. Both subsystems, the QD and the superconducting electrons, are coupled via the tunneling or hybridization term,

$$H_t = \sum_{k,p,\sigma} t_p (d^\dagger_\sigma c_{k,p,\sigma} + \text{H.c.}), \tag{4}$$

where t_p is the matrix element of tunneling between the QD and the p lead. Our aim here is to set up the simplest model that still retains the essential features of the interplay between the Josephson current and Kondo effect. To this end, following our previous work [28], and the work by Vecino *et al.* [29] and Bergeret *et al.* [30], by integrating out the electronic degrees of freedom of the superconducting leads [31], we can obtain a simplified model Hamiltonian $\tilde{H}_s$ to describe the superconducting leads given by

$$\tilde{H}_s = -\Delta (e^{i\varphi/2} c^\dagger_{L\uparrow} c^\dagger_{L\downarrow} + e^{-i\varphi/2} c^\dagger_{R\uparrow} c^\dagger_{R\downarrow} + \text{H.c.}), \tag{5}$$

where Δ is an effective pairing potential in the leads and $c^\dagger_{L(R)\sigma}$ ($c_{L(R)\sigma}$) creates (destroys) an electron in the lead $L(R)$ with spin σ. In Eq. (5) we have taken the Fermi energy in the leads as the origin of energies. Following this approach, we take an effective Hamiltonian to describe the coupling between the QD and the leads given by

$$\tilde{H}_t = \sum_{p,\sigma} t (d^\dagger_\sigma c_{p,\sigma} + \text{H.c.}), \tag{6}$$

where t is an effective hybridization parameter. With this approximation an effective "narrow-band" Hamiltonian for the system is obtained:

$$\tilde{H} = \tilde{H}_s + H_d + \tilde{H}_t. \tag{7}$$

This simplification prevents us from making a quantitative comparison with experiments. However, as we will see, the qualitative conclusions of our model are physically valid, the conceptual ingredients remain intact, and the physics involved is transparent. Before we proceed with the study of the physical properties of $\tilde{H}$, it is useful to define new leads operators: $\alpha^\dagger_\sigma := (c^\dagger_{L\sigma} + c^\dagger_{R\sigma})/\sqrt{2}$ and $\gamma^\dagger_\sigma := (c^\dagger_{L\sigma} - c^\dagger_{R\sigma})/\sqrt{2}$. Thus $\tilde{H}_t$ can be written as

$$\tilde{H}_t = \sum_\sigma \sqrt{2} t \left(d^\dagger_\sigma \alpha_\sigma + \text{H.c.} \right). \tag{8}$$

Only lead symmetric operators α_σ and $\alpha^\dagger_\sigma$ couple directly to the dot, through an enhanced tunneling matrix element $\sqrt{2}\,t$. The $\tilde{H}_s$, in terms of the new operators, reads

$$\begin{aligned} \tilde{H}_s = &-\Delta \{ \cos(\varphi/2) [\alpha^\dagger_\uparrow \alpha^\dagger_\downarrow + \gamma^\dagger_\uparrow \gamma^\dagger_\downarrow + \text{H.c.}] \\ &+ \sin(\varphi/2) [i(\alpha^\dagger_\uparrow \gamma^\dagger_\downarrow - \alpha^\dagger_\downarrow \gamma^\dagger_\uparrow) + \text{H.c.}] \}. \end{aligned} \tag{9}$$

Finally, when the parameters U, ε_d, and t are such that the QD level occupation approaches one, it is possible to describe the physics of the system with a reduced Hamiltonian that couples *only* the QD spin to the leads [32,33]. This reduced Hamiltonian includes an antiferromagnetic (Kondo) interaction between QD and superconducting spins. In this limit, the contribution from $H_d + \tilde{H}_t$ in Eq. (7) may be

approximated by the Kondo interaction

$$\tilde{H}_K = \frac{J}{2}(s_\alpha^+ S_d^- + s_\alpha^- S_d^+) + J s_\alpha^z S_d^z, \tag{10}$$

where $s_\alpha^+ = \alpha_\uparrow^\dagger \alpha_\downarrow$, $s_\alpha^- = \alpha_\downarrow^\dagger \alpha_\uparrow$, $s_\alpha^z = (\alpha_\uparrow^\dagger \alpha_\uparrow - \alpha_\downarrow^\dagger \alpha_\downarrow)/2$, J $(= 4t^2/|\varepsilon_d|) > 0$ is an effective antiferromagnetic coupling between the dot and the leads, and the different components of the dot spin $S = 1/2$ read $S_d^+ = d_\uparrow^\dagger d_\downarrow$, $S_d^- = d_\downarrow^\dagger d_\uparrow$, and $S_d^z = (d_\uparrow^\dagger d_\uparrow - d_\downarrow^\dagger d_\downarrow)/2$. The limit $U \to \infty$ has been taking in obtaining Eq. (10), preventing strictly the dot double occupancy [32,33]. Thus, in the Kondo regime of the QD, an effective model Hamiltonian for the system is obtained

$$\tilde{H} = \tilde{H}_s + \tilde{H}_K. \tag{11}$$

The Hilbert space corresponding to the Hamiltonian given by Eq. (11) comprises just 32 states, corresponding to the four possible occupations (0, ↑, ↓, and ↑↓) of each lead and the two occupations (↑, ↓) of the dot. This space can be written as follows: (I) one-particle (dot) states (2): $|\sigma\rangle = d_\sigma^\dagger|0\rangle$ (with $|0\rangle$ the vacuum state); (II) two-particle states (8): $\alpha_{\sigma'}^\dagger|\sigma\rangle$ and $\gamma_{\sigma'}^\dagger|\sigma\rangle$; (III) three-particle states (12): $\alpha_\uparrow^\dagger\alpha_\downarrow^\dagger|\sigma\rangle$, $\gamma_\uparrow^\dagger\gamma_\downarrow^\dagger|\sigma\rangle$, and $\alpha_{\sigma'}^\dagger\gamma_{\sigma''}^\dagger|\sigma\rangle$; (IV) four-particle states (8): $\alpha_\uparrow^\dagger\alpha_\downarrow^\dagger\gamma_{\sigma'}^\dagger|\sigma\rangle$ and $\gamma_\uparrow^\dagger\gamma_\downarrow^\dagger\alpha_{\sigma'}^\dagger|\sigma\rangle$; (V) five-particle states (2): $\alpha_\uparrow^\dagger\alpha_\downarrow^\dagger\gamma_\uparrow^\dagger\gamma_\downarrow^\dagger|\sigma\rangle$. Note that the subspaces with even (2,4) and odd (1,3,5) number of electrons are mixed to be the superconducting Hamiltonian $\tilde{H}_s$. Nevertheless, the exact solution of the problem reduces to the diagonalization of one 4×4 and four 2×2 matrices as the full Hilbert space is drastically block diagonalized. From the eigenvalues, the partition function is calculated from which the analytical expression for the free energy and the associated Josephson current as a function of the parameters is immediately obtained. Since the zero-temperature results presented in the first part of the next section are for the Kondo-limit Hamiltonian $\tilde{H}$ of Eq. (11), this prevents us from a quantitative comparison with the zero-temperature results of Refs. [29] and [30], corresponding to the more general model of Eq. (7). The results from the two models agree, of course, once the parameters U, ε_d, and t of the latter are tuned towards the Kondo limit, as explained above Eq. (10).

The narrow-band or "zero-bandwidth" approximation leading to our effective hybrid superconductor-quantum dot Hamiltonian of Eq. (7) has been applied successfully to study a variety of different problems in the past years. Introduced first in the context of valence fluctuating problems [34–36] and for the study of the effect of magnetic impurities in superconducting matrices [37,38] has been applied later to the study of the electrical transport properties of semiconductor quantum dots [28], and also to calculate the magnetic correlations between two-magnetic impurities in a metallic matrix [39]. In all cases, this simple approach has been in good qualitative agreement with more elaborate theoretical approaches, and provided a transparent physical view of complicated many-body problems, like the Kondo effect. The combination of simplicity and right physics motivate also some authors to discuss the narrow-band limit or zero-bandwidth model in several textbooks [40–42].

III. RESULTS AND DISCUSSION

A. Zero temperature

At zero temperature, the model is completely characterized by the dimensionless parameter (Δ/J) and the phase φ which is determined by looking for the minimum of the ground-state energy. As we will see, for any value of (Δ/J), this minimum corresponds either to $\varphi = 0$ or $\varphi = \pi$.

There is a critical value $\Delta = \Delta_c = (1 + \sqrt{17})J \simeq 0.64J$ (to be derived below) below which (i.e., for $\Delta < \Delta_c$) the localized magnetic moment in the QD is screened by the Kondo effect, and the ground state is a spin singlet. This regime corresponds to $\varphi = 0$ and it is known as the 0 or 0′ junction regime (see below). The singlet ground-state energy of $\tilde{H}$ and the corresponding eigenvector can be obtained easily from the lowest eigenvalue of the following 2×2 matrix:

$$\begin{vmatrix} -3J/4 - \Delta\cos(\varphi/2) - \lambda & \Delta\sin(\varphi/2) \\ \Delta\sin(\varphi/2) & \Delta\cos(\varphi/2) - \lambda \end{vmatrix} = 0. \tag{12}$$

The solution is trivial and we obtain

$$\lambda_{0,1}(\varphi) = -\frac{3J}{8}[1 + R_{3,1}(\varphi)], \tag{13}$$

with

$$R_{m,n}(\varphi) = \sqrt{1 - (-1)^n \frac{16\Delta}{mJ}\cos(\varphi/2) + \frac{64\Delta^2}{(mJ)^2}} \tag{14}$$

for $0 \leqslant \varphi \leqslant \pi$ and $R_{m,1}(\varphi) > R_{m,2}(\varphi)$. The eigenvalues are denoted by $\lambda_{S,i}(\varphi)$, with the first index either $S = 0$ (singlet), $S = 1/2$ (doublet), or $S = 1$ (triplet). The second index just enumerates the S-type solutions in ascending order ($i = 1$, the ground state).

The corresponding eigenvector associated with the eigenvalue (13) is given by

$$\begin{aligned} |0,1\rangle(\varphi) = {} & a_1(\varphi)\frac{1}{\sqrt{2}}(1 + \gamma_\uparrow^\dagger\gamma_\downarrow^\dagger)\frac{1}{\sqrt{2}}(\alpha_\uparrow^\dagger|\downarrow\rangle - \alpha_\downarrow^\dagger|\uparrow\rangle) \\ & + a_2(\varphi)\frac{i}{\sqrt{2}}(-1 + \alpha_\uparrow^\dagger\alpha_\downarrow^\dagger)\frac{1}{\sqrt{2}}(\gamma_\uparrow^\dagger|\downarrow\rangle - \gamma_\downarrow^\dagger|\uparrow\rangle), \end{aligned} \tag{15}$$

where

$$a_1(\varphi) = \frac{1}{\sqrt{2}}\left[1 + \frac{1 + 8\Delta\cos(\varphi/2)/(3J)}{R_{3,1}(\varphi)}\right]^{1/2} \tag{16}$$

and

$$a_2(\varphi) = -\frac{1}{\sqrt{2}}\left[1 - \frac{1 + 8\Delta\cos(\varphi/2)/(3J)}{R_{3,1}(\varphi)}\right]^{1/2}. \tag{17}$$

For $\varphi = 0$, $a_1(0) = 1$, $a_2(0) = 0$, Eq. (13) gives the lowest eigenvalue $\lambda_{0,1}(0) = -3J/4 - \Delta$, and the ground state reduces to

$$|0,1\rangle(0) = \frac{1}{\sqrt{2}}(1 + \gamma_\uparrow^\dagger\gamma_\downarrow^\dagger)\frac{1}{\sqrt{2}}(\alpha_\uparrow^\dagger|\downarrow\rangle - \alpha_\downarrow^\dagger|\uparrow\rangle). \tag{18}$$

$|0,1\rangle(0)$ shows the product of two independent subspaces: only the α fermions are coupled to the electron in the

dot and produce a singlet state. That is, in simplified terms, the physics that governs the Kondo effect in the QD. The other factor (γ fermions) represents the superconductivity in the leads as a mixing of zero and two electrons with opposite spins. The weight of the second component with coefficient $a_2(\varphi)$ increases by increasing φ from zero, but always is fulfilled that $a_1(\varphi) \geqslant |a_2(\varphi)|$.

For $\Delta > \Delta_c$, the ground state is a doublet characterized by a reversal of the sign of the Josephson current-phase relation ($\varphi_L - \varphi_R = \pi$), this is the π-junction regime and the minimum ground-state energy corresponds to $\varphi = \pi$. The ground state can be obtained from the lowest eigenvalue $\lambda_{1/2,1}(\varphi)$ and the corresponding eigenvector $[b_1(\varphi), b_2(\varphi), b_3(\varphi), b_4(\varphi)]$ of a 4×4 matrix, given by

$$\begin{vmatrix} -J/2-\lambda & \sqrt{3}J/4 & 0 & 0 \\ \sqrt{3}J/4 & -\lambda & 2\Delta\,\sin(\varphi/2) & 0 \\ 0 & 2\Delta\,\sin(\varphi/2) & -\lambda & -2\Delta\,\cos(\varphi/2) \\ 0 & 0 & -2\Delta\,\cos(\varphi/2) & -\lambda \end{vmatrix} = 0. \tag{19}$$

For $\varphi = \pi$, we obtain the ground-state energy $\lambda_{1/2,1}(\pi)$, and we can write the doublet ground state as

$$\begin{aligned} |1/2,1\rangle(\pi) = {} & \frac{b_1}{\sqrt{6}}[(\alpha_\uparrow^\dagger \gamma_\downarrow^\dagger + \alpha_\downarrow^\dagger \gamma_\uparrow^\dagger)|\sigma\rangle - 2\alpha_\sigma^\dagger \gamma_\sigma^\dagger |\overline{\sigma}\rangle] \\ & + \frac{b_2}{\sqrt{2}}(\alpha_\uparrow^\dagger \gamma_\downarrow^\dagger - \alpha_\downarrow^\dagger \gamma_\uparrow^\dagger)|\sigma\rangle \\ & + \frac{ib_3}{\sqrt{2}}(1 + \alpha_\uparrow^\dagger \alpha_\downarrow^\dagger \gamma_\uparrow^\dagger \gamma_\downarrow^\dagger)|\sigma\rangle \\ & + \frac{ib_4}{\sqrt{2}}(\alpha_\uparrow^\dagger \gamma_\downarrow^\dagger + \alpha_\downarrow^\dagger \gamma_\uparrow^\dagger)|\sigma\rangle, \end{aligned} \tag{20}$$

where $b_1 = b_1(\pi)$, $b_2 = b_2(\pi)$, $b_3 = b_3(\pi)$, and $b_4 = b_4(\pi) = 0$. The first term in $|1/2,1\rangle(\pi)$ gives the contribution due to the antiferromagnetic coupling (Kondo) between the spin $S = 1$ in the leads and the spin $S = 1/2$ in the dot and it represents the contribution of the Kondo effect in the π regime. When Δ is increased this term goes to zero. On the contrary, the second and third term involves the unscreened spin 1/2 in the dot. The second term shows the electrons in the leads in a superconducting singlet state and $|b_2|^2 \to 1/2$ for large values of Δ. Finally, the third term represents a superconducting contribution and it increases when Δ is increased from the Δ_c ($|b_3|^2 \to 1/2$). Therefore, for $\Delta \gg \Delta_c$, from Eq. (19) we obtain $\lambda_{1/2,1}(\pi) \simeq -2\Delta - 3J^2/(64\Delta)$ and the ground state can be approximated by $b_1 \simeq -\sqrt{3}J(1 + 0.25J/\Delta)/(8\sqrt{2}\Delta)$, $b_2 \simeq 1/\sqrt{2}$, and $b_3 \simeq [-1 + 3J^2/(128\Delta^2)]/\sqrt{2}$. From the "crossing" condition $\lambda_{1/2,1}(\pi) = \lambda_{0,1}(0) = -3J/4 - \Delta$, the analytical expression of Δ_c can be obtained exactly as $\Delta_c = J(1 + \sqrt{17})/8 \simeq 0.64J$.

In Fig. 1, we show the φ dependence of eigenvalues $\lambda_{S,i}(\varphi)$, with $S = 0$, $S = 1/2$, and $S = 1$, for $\Delta/J = \Delta_c/J$. For $S = 0$ (full lines) they are given in ascending ordering by Eq. (13) and $\lambda_{0,2}(\varphi) = -3J/8[1 + R_{3,2}(\varphi)]$, $\lambda_{0,3}(\varphi) = -3J/8[1 - R_{3,2}(\varphi)]$, and $\lambda_{0,4}(\varphi) = -3J/8[1 - R_{3,1}(\varphi)]$. For $S = 1/2$ the figure shows (dashed lines) the four eigenvalues of Eq. (19) [$\lambda_{1/2,i}(\varphi)$ for $i = 1,2,3,4$]. For $S = 1$ (dotted lines) the analytical expressions for the displayed eigenvalues are $\lambda_{1,1}(\varphi) = J/8[1 - R_{1,1}(\varphi)]$, $\lambda_{1,2}(\varphi) = J/8[1 - R_{1,2}(\varphi)]$, $\lambda_{1,3}(\varphi) = J/8[1 + R_{1,2}(\varphi)]$, and $\lambda_{1,4}(\varphi) = J/8[1 + R_{1,1}(\varphi)]$.

Considering spin degeneracies, altogether 24 eigenvalues are shown in Fig. 1 (4 belonging to singlet states, 8 corresponding to doublet states, and 12 belonging to triplet states). The remaining eight eigenvalues are independent of φ, and they do not become the ground state for the range of parameters used in this work. It is interesting to note that for exactly this particular value of Δ, $\lambda_{0,1}(0) = \lambda_{1/2,1}(\pi)$, which marks the zero-temperature boundary between the junction 0like behavior ($\Delta < \Delta_c$) to the junction π-like behavior ($\Delta > \Delta_c$). Some useful symmetry properties of the eigenvalues are as follows. Defining $\varphi' = \pi - \varphi$, the eigenvalues of the 4×4 matrix of Eq. (19) satisfy $\lambda_{1/2,i}(\varphi') = \lambda_{1/2,i}(-\varphi')$. This is easily proved by checking that the quartic equation for the λ's that results from Eq. (19) remains invariant

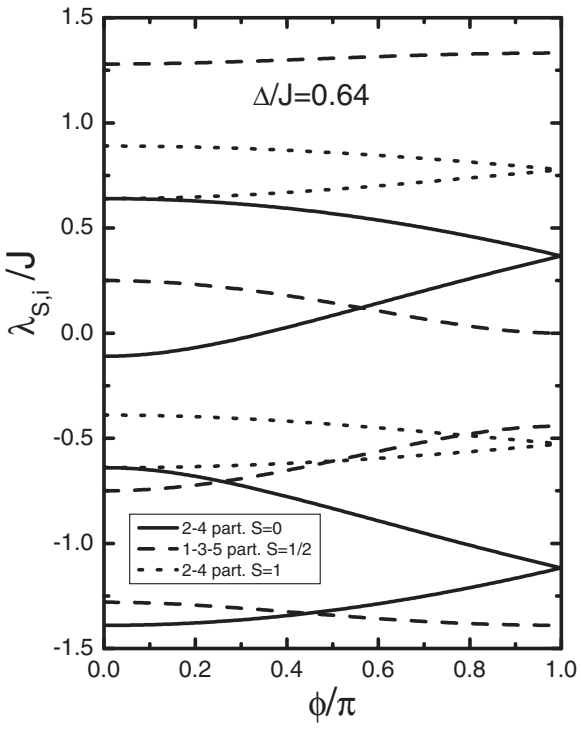

FIG. 1. φ dependence of eigenvalues $\lambda_{S,i}(\varphi)$, with $S = 0$, $S = 1/2$, and $S = 1$, for $\Delta/J = 0.64$. For each Δ, the point of intersection between the two lowest eigenvalues, $\lambda_{0,1}(\varphi^*) = \lambda_{1/2,1}(\varphi^*)$, defines $\varphi^*(\Delta)$. For this particular case, $\varphi^*(\Delta = \Delta_c) \sim 0.45\pi$. For $\Delta/J = 0.75$ (not shown), $\varphi^* = 0$, and $\lambda_{0,1}(0) = \lambda_{1/2,1}(0)$; for $\Delta/J > 0.75$ (not shown), $\lambda_{0,1}(\varphi) > \lambda_{1/2,1}(\varphi)$ for all φ.

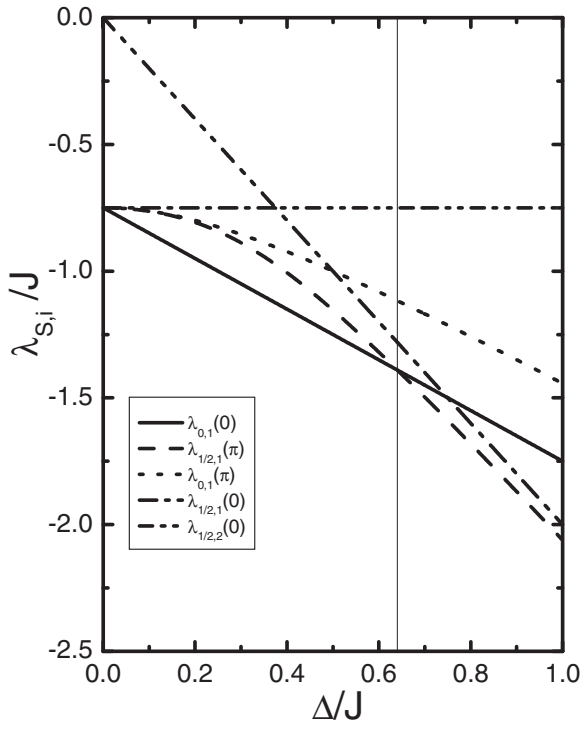

FIG. 2. Lowest energy levels of $\tilde{H}$ as a function of Δ/J. For $\Delta < \Delta_c \simeq 0.64J$ we can observe the singlet (solid line) ground-state energy $\lambda_{0,1}(0)$, and for $\Delta > \Delta_c$ the doublet (dashed line) ground-state energy $\lambda_{1/2,1}(\pi)$ is observed. The thin vertical line denotes the transition point.

under the change $\varphi' \to -\varphi'$. On the other side, using the analytical expressions for the singlet states, it results that $\lambda_{0,1}(\varphi') = \lambda_{0,2}(-\varphi')$, and that $\lambda_{0,3}(\varphi') = \lambda_{0,4}(-\varphi')$. In brief, the full spectrum shown in Fig. 1 is invariant under the change $\varphi' \to -\varphi'$. In Fig. 9 of Ref. [22], the first and second many-body excited states of the full model given by Eq. (1) have been obtained, using the NRG. Looking at the corresponding low-energy region of the full spectrum in Fig. 1, the similarity is quite encouraging. The results in Ref. [22] are, however, for finite U.

In Fig. 2, we show the lowest energy levels $\lambda_{S,i}(\varphi)$ of Fig. 1, for $\varphi = 0$, and π, as a function of Δ/J. The figure shows $\lambda_{0,1}(0) = -3J/4 - \Delta$, the eigenvalue of $|0,1\rangle(0)$, $\lambda_{1/2,1}(\pi)$, the eigenvalue of $|1/2,1\rangle(\pi)$, $\lambda_{0,1}(\pi) = -3J/8 - \sqrt{9J^2/64 + \Delta^2}$, $\lambda_{1/2,1}(0)$, and $\lambda_{1/2,2}(0)$. The analytical expressions for these two last eigenvalues are

$$\lambda_{1/2,1}(0) = -\frac{3J}{4}\theta\left(0.375 - \frac{\Delta}{J}\right) - 2\Delta\theta\left(\frac{\Delta}{J} - 0.375\right) \tag{21}$$

and

$$\lambda_{1/2,2}(0) = -\frac{3J}{4}\theta\left(\frac{\Delta}{J} - 0.375\right) - 2\Delta\theta\left(0.375 - \frac{\Delta}{J}\right). \tag{22}$$

Here, $\theta(x) = 1$ if $x > 0$, and $\theta(x) = 0$ if $x < 0$. It is interesting to observe at this point that at $\Delta = 0.75J$, $\lambda_{0,1}(0) = \lambda_{1/2,1}(0)$; this marks the zero-temperature boundary between the π- and π'-junction behavior (see below). In other words, for $\Delta/J > 0.75$, $\lambda_{1/2,1}(\varphi)$ is the ground state of the system for any value of φ.

It is instructive at this point to compare the results displayed in Figs. 1 and 2 with the equivalent results displayed in Figs. 4 and 5 of Ref. [29], for the same narrow-band model, but for finite U. The link between both models is given by the antiferromagnetic Kondo coupling for finite U,

$$J(U) = \frac{4t^2U}{|\varepsilon_d|(U + \varepsilon_d)}, \tag{23}$$

which for $U \gg |\varepsilon_d|$ coincides with the expression given before, $J(U \to \infty) \to J = 4t^2/|\varepsilon_d|$. In some sense, the three parameters involved in the calculations of Ref. [29] (t, U, ε_d), are collapsed in a single parameter $J(U)$ in Eq. (23), which for large U coincides with our J. First note that for $t/\Delta = 1.2$ and $\varepsilon_d/\Delta = -10$ (parameters corresponding to Fig. 4 in Ref. [29]), $J = 4t^2/|\varepsilon_d| = 0.576\Delta \to \Delta/J \simeq 1.74$. And since for this value of the unique parameter Δ/J (in our model) the system is well inside the π-phase regime, it may be expected that as U increases, the system of Ref. [29] progressively enters in this regime. This is exactly the tendency observed in Fig. 4 of Ref. [29]: for example, panel (d), corresponding to $U/\Delta = 18$, has a value of $\Delta/J(U) \simeq 0.77$, just above the threshold value of 0.75 found in our case for having a π-type ground state for any value of φ (see caption in Fig. 1). Passing to the results in Fig. 5 of Ref. [29], from Eq. (23) we obtain that $\Delta/J(U) \simeq 0.11$ for panel (a), and that $\Delta/J(U) \simeq 0.43$ for panel (b). According to our model, for small values of Δ/J the crossing point $\varphi^*(\Delta/J)$ is close to π, as observed in panel (a). On the other side, for $\Delta/J \simeq 0.43$ the system is in the $0'$ phase, as observed in panel (b). Regarding the zero-temperature "phase diagram" displayed in Fig. 6 of Ref. [29], the same is out of the reach for our model, as a result of working in the large-U (infinite) Kondo limit.

The Josephson current $I(\varphi)$ through the quantum dot can be obtained using $I(\varphi) = (2e/\hbar)dF(\varphi)/d\varphi$, where $F(\varphi)$ is the free energy of the system. At zero temperature, the free energy becomes the ground-state energy, and for $0 \leqslant \varphi \leqslant \varphi^*(\Delta)$, from Eq. (13) it is straightforward to obtain the analytical expression

$$\frac{I_0(\varphi)}{I_0} = \left[1 + \frac{16\Delta}{3J}\cos\left(\frac{\varphi}{2}\right) + \frac{64\Delta^2}{9J^2}\right]^{-1/2}\sin\left(\frac{\varphi}{2}\right), \quad \geqslant 0, \tag{24}$$

while, for $\varphi^*(\Delta) \leqslant \varphi \leqslant \pi$,

$$\frac{I_\pi(\varphi)}{I_0} = \frac{3\Delta}{16JA_1(\varphi)}\sin(\varphi) \leqslant 0, \tag{25}$$

with

$$A_i(\varphi) = \bar{\lambda}^3_{1/2,i}(\varphi) + \frac{3}{8}\bar{\lambda}^2_{1/2,i}(\varphi) - \frac{3J^2 + 64\Delta^2}{32J^2}\bar{\lambda}_{1/2,i}(\varphi) - \frac{\Delta^2}{2J^2}. \tag{26}$$

Here $I_0 = e\Delta/\hbar$ is the critical current of a transparent single-mode junction, $\bar{\lambda}_{1/2,i}(\varphi) = \lambda_{1/2,i}(\varphi)/J$, and $\varphi^*(\Delta/J)$ is defined, for each Δ, as the intersection point between the two lowest eigenvalues, $\lambda_{0,1}(\varphi^*) = \lambda_{1/2,1}(\varphi^*)$ (see Fig. 1). In

obtaining Eq. (25), the quartic equation resulting from Eq. (19) has been used, for the direct evaluation of $d\lambda_{1/2,1}(\varphi)/d\varphi$. From Eqs. (25) and (19), it is easy to prove that $I_\pi(\varphi - \pi/2) = I_\pi(\pi/2 - \varphi)$, and then that $I_\pi(\varphi)$ has an extremum at $\varphi = \pi/2$; in consequence $I_\pi(\pi/2)$ is the minimum possible value of $I_\pi(\varphi)$.

The signs of $I_0(\varphi)$ and $I_\pi(\varphi)$ are opposite, and this is the most distinctive feature that distinguishes the 0 junction from the π-junction regime. The difference in sign is evident from the opposite slopes in Fig. 1 of $\lambda_{0,1}(\varphi)$ and $\lambda_{1/2,1}(\varphi)$, and also from the analytical expressions in Eqs. (24) and (25). From a more microscopic point of view, the positive slope of $\lambda_{0,1}(\varphi)$ comes from the fact that the gain in energy for the singlet ground state is optimum for $\varphi = 0$. From Eq. (18), it is quite clear that in $|0,1\rangle(0)$ the α electrons are fully devoted to build the Kondo singlet, while the γ electrons are exclusively involved in the superconductivity. Increasing φ, $a_2(\varphi) \neq 0$ and both α and γ electrons are involved in building the Kondo singlet. But as the γ electrons are not directly coupled to the QD, the gain in energy is smaller. For $\varphi = \pi$, from Eq. (9) is clear that the superconductivity is only possible for "mixed" α-γ pairs, and this is in direct conflict with the Kondo singlet. Regarding the negative slope of $\lambda_{1/2,1}(\varphi)$, from Eq. (21), $\lambda_{1/2,1}(0) = -2\Delta$; in this configuration, all gain in energy comes from the superconductivity, with zero Kondo contribution. Increasing φ, $\lambda_{1/2,1}(\varphi)$ gain energy both from the superconductivity and by the Kondo effect, and the energy decreases. For $\varphi = \pi$, the ground state is $|1/2,1\rangle(\pi)$ in Eq. (20): the mixed pairs α-γ found the way to contribute both to the superconductivity (term proportional to b_2), and to a kind of spin-1 Kondo effect (term proportional to b_1).

Depending on the value of Δ/J, four zero-temperature configurations are then (in principle) possible for the junction.

(a) $\varphi^*(\Delta/J) = \pi$, and the Josephson current is given by Eq. (24) for $0 \leqslant \varphi \leqslant \pi$. This is the 0-junction regime, which is not realized for any finite value of Δ. One way to see this is from the very same Eq. (24), according to which $I_0(\pi)/I_0 \neq 0$, and this is not possible.

(b) $0 < \varphi^*(\Delta/J) < \pi$, with $\lambda_{0,1}(0) < \lambda_{1/2,1}(\pi)$. This is the $0'$-junction regime, valid for $\Delta < \Delta_c$.

(c) $0 < \varphi^*(\Delta/J) < \pi$, but $\lambda_{0,1}(0) > \lambda_{1/2,1}(\pi)$. This is the π'-junction regime, valid for $\Delta_c < \Delta < 0.75J$.

(d) $\varphi^*(\Delta/J) = 0$, and the Josephson current is given by Eq. (25) for $0 \leqslant \varphi \leqslant \pi$. This is the π-junction regime, and it is realized for $\Delta/J \geqslant 0.75$.

The Josephson current is *positive* both in the 0- and $0'$-junction regimen, and *negative* in the π and π'-junction regime.

It is important to note that in the $0'$- and π'-junction configurations the Josephson current is given by two different functions at right and left of $\varphi^*(\Delta/J)$, which gives rise to a discontinuity given by

$$\Delta I_{0-\pi}[\varphi^*(\Delta/J)] := I_0[\varphi^*(\Delta/J)] - I_\pi[\varphi^*(\Delta/J)] > 0. \tag{27}$$

This is shown in Fig. 3. For $\Delta \gg \Delta_c$, $\lambda_{1/2,1}(\varphi) \to -2\Delta - 3J^2 \sin^2(\varphi/2)/(64\Delta)$. Evaluation of $A_i(\varphi)$ in Eq. (26) with this approximation for $\lambda_{1/2,1}(\varphi)$, and replacing in Eq. (25),

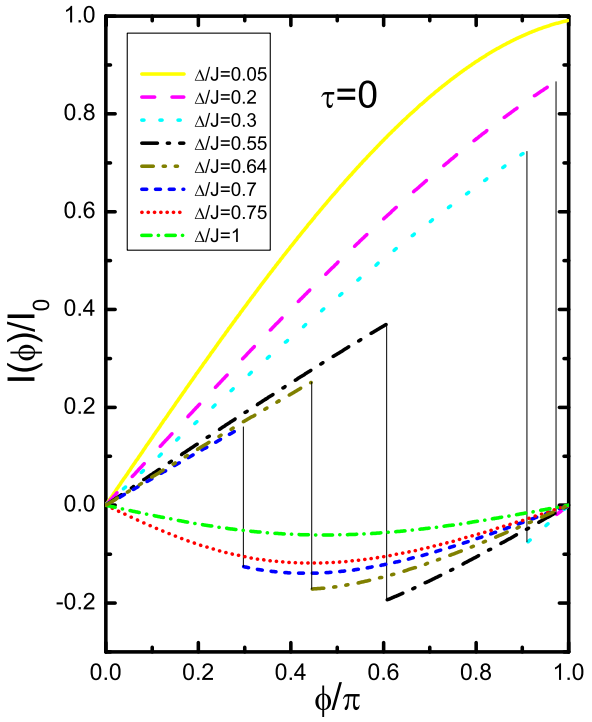

FIG. 3. (Color online) Zero-temperature Josephson current $I(\varphi)/I_0$ as a function of φ, for different values of Δ/J. All curves, except the ones for $\Delta/J = 0.75$ and 1, have a discontinuity at $\varphi^*(\Delta)$, indicated by the vertical thin straight line. The size of the discontinuity is given by Eq. (27). $\tau = k_B T$.

yields the leading contribution

$$\frac{I_\pi(\varphi)}{I_0} \approx -\frac{3J^2}{64\Delta^2}\sin(\varphi). \tag{28}$$

This equation describes the zero-temperature Josephson current well inside the π-junction regime. The zero-temperature results displayed in Fig. 3 look quite similar to the ones in Fig. 4 of Ref. [22], obtained using both the FRG and the NRG for the full model, and for finite U.

Since the discontinuity in $I(\varphi)/I_0$ displayed in Fig. 3 is exactly located at $\varphi^*(\Delta/J)$, from here it is possible to follow the evolution of $\varphi^*(\Delta/J)$ for increasing values of Δ/J. For small values of this parameter, $\varphi^*(\Delta/J) \sim \pi$, and then it decreases monotonically as Δ/J increases, reaching zero when $\Delta/J = 0.75$. For larger values of Δ/J, the junction is in the π regime, and $\varphi^*(\Delta/J) = 0$.

Zero-temperature $I(\varphi)/I_0$ vs φ diagrams have been obtained previously through the solution of the full standard model of Eq. (1) [22]. The similarity with the results presented in Fig. 3 is remarkable. This gives the first hint of what is one of the messages of the present work: that besides the drastic simplification introduced by the narrow-band approximation, after it the model still retains all the important physical ingredients of the original model, reproducing in a qualitative way their results. This conclusion is extended to the finite-temperature case in the following section.

B. Finite temperature

At finite temperatures, it is straightforward to obtain the free energy of the system as a function of the model parameters. We can write $F(\varphi) = -k_B T \ln[Z(\varphi)]$, with $Z(\varphi)$ the partition function given by

$$Z(\varphi) = 2\exp\left(\frac{3\beta J}{8}\right)\sum_{n=1}^{2}\cosh[3\beta J R_{3,n}(\varphi)/8] + 6\exp\left(-\frac{\beta J}{8}\right)\sum_{n=1}^{2}\cosh[\beta J R_{1,n}(\varphi)/8] + 2\sum_{i=1}^{4}\exp[-\beta\lambda_{1/2,i}(\varphi)] + 4\left[1+\exp\left(-\frac{\beta J}{4}\right)\right], \tag{29}$$

where $\beta = 1/(k_B T)$, k_B being the Boltzmann constant. The first and the second terms in $Z(\varphi)$ give the contribution due to the mixing of two-particle and four-particle states with total spin $S = 0$ and $S = 1$, respectively. The third term gives the contribution of eigenvalues of Eq. (19). Finally, the last term gives the contribution of four states of $S = 1/2$ and zero energy corresponding to $\frac{1}{\sqrt{2}}(\alpha_\uparrow^\dagger\alpha_\downarrow^\dagger - \gamma_\uparrow^\dagger\gamma_\downarrow^\dagger)|\sigma\rangle$ and $\frac{1}{\sqrt{2}}(1-\alpha_\uparrow^\dagger\alpha_\downarrow^\dagger\gamma_\uparrow^\dagger\gamma_\downarrow^\dagger)|\sigma\rangle$, and other four three-particle states with $S = 3/2$ and energy $J/4$. Being independent of φ, these eight states play no role in what follows. Since the full energy spectra is invariant under the change $\varphi' \to -\varphi'$, $F(\pi-\varphi) = F(\varphi-\pi)$, and $F(\varphi)$ enters with zero slope at $\varphi \to \pi$.

In Fig. 4 we show $F(\varphi)$ as a function of φ, for $\tau/J = 0.01$, and different values of Δ/J. Depending on the value of Δ/J, we can observe two different absolute minimum of the free energy either at $\varphi = 0$ or π, and one maximum at $0 < \varphi < \pi$. In the region of parameters where this maximum exists, it allows us to identify the finite temperature $0'$-junction regime when the absolute minimum of $F(\varphi)$ corresponds to $\varphi = 0$, and the π'-junction finite-temperature behavior when the absolute minimum of $F(\varphi)$ occurs at $\varphi = \pi$ [20]. For small values of Δ/J, $F(\varphi)$ shows the 0-junction behavior, the physics is dominated by the Kondo effect, and we can see the minimum of $F(\varphi)$ at $\varphi = 0$, with a weak dependence of φ (see solid line for $\Delta/J = 0.1$). Increasing Δ/J the maximum at $\varphi = \pi$ moves up ($\Delta/J = 0.2, 0.3$). For $\Delta/J \simeq 0.306$, the free energy shows the transition from the 0-junction to $0'$-junction behavior, and for $0.306 \lesssim \Delta/J \lesssim 0.631$ the $0'$-junction behavior can be observed ($\Delta/J = 0.35, 055$). For $\Delta/J \simeq 0.631$, where $F(\varphi = 0) \simeq F(\varphi = \pi)$, the model gives the transition from $0'$ to π' behavior. For $0.631 \lesssim \Delta/J \lesssim 0.744$, the free energy corresponding to the π'-junction behavior can be observed ($\Delta/J = 0.64, 0.70$). Finally, for $\Delta/J \simeq 0.744$ the transition from π' to π junction takes place and the figure shows the π-junction behavior of the free energy for $\Delta/J = 0.75$.

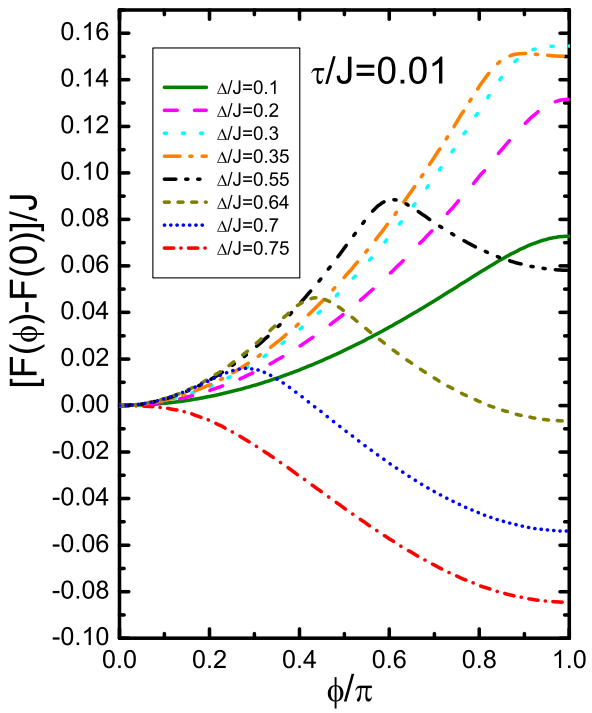

FIG. 4. (Color online) Free energy $F(\varphi)$ as a function of φ [measured from $F(\varphi = 0)$], for $\tau/J = 0.01$ and different values of Δ/J. $F(\varphi)$ enters with zero slope at the limiting values $\varphi = 0, \pi$.

From the free energy it is easy to write the Josephson current explicitly as

$$\frac{I(\varphi)}{I_0} = \frac{\sin(\varphi/2)}{Z(\varphi)}\left\{2\exp(3\beta J/8)\sum_{n=1}^{2}\frac{\sinh[3\beta J R_{3,n}(\varphi)/8]}{(-1)^{n-1}R_{3,n}(\varphi)} + 6\exp(-\beta J/8)\sum_{n=1}^{2}\frac{\sinh[\beta J R_{1,n}(\varphi)/8]}{(-1)^{n-1}R_{1,n}(\varphi)} + \frac{3\Delta}{8J}\cos(\varphi/2)\sum_{i=1}^{4}\frac{\exp[-\beta\lambda_{1/2,i}(\varphi)]}{A_i(\varphi)}\right\}. \tag{30}$$

From Eq. (30) we obtain $I(0) = I(\pi) = 0$. The fact that $I(0) = 0$ is explicit from the equation above. On the other side, $I(\pi) = 0$ is a consequence of the symmetry properties of the eigenvalues under the change $\varphi'(=\pi-\varphi) \to -\varphi'$ discussed previously.

In Fig. 5, we can see the φ dependence of the Josephson current through the QD for $\tau/J = 0.01$ and Δ/J ranging from 0.05 to 1. Three types of behavior can be observed: (I) for small values of Δ/J, the 0-junction regime, where the Kondo physics is important and the current is positive ($\Delta/J = 0.05$, 0.10, 0.20, and 0.30), (II) the crossover regime ($0'$ and π' junction), for $\Delta/J = 0.55$ and 0.70, where the current shows positive and negative values, and (III) the π-junction regime, where the current is negative, has a sinusoidal behavior, and is small (see $\Delta/J = 0.75$ and 1). These results are in a good qualitative agreement with the results obtained in Ref. [20] using Monte Carlo simulations [43]. Comparison between the zero-temperature and finite-temperature results of Figs. 3 and 5, respectively, reveals how the zero-temperature discontinuities $\Delta I_{0-\pi}[\varphi^*(\Delta/J)]$ are transformed in broadened transitions, located essentially at the same $\varphi^*(\Delta/J)$. At difference with the $T = 0$ results, however, the maximum in $I(\varphi)/I_0$ shows a nonmonotonic behavior with increasing Δ, first increasing ($0.05 \to 0.10$), and then decreasing ($0.10 \to 0.20 \to 0.30 \to 0.55$).

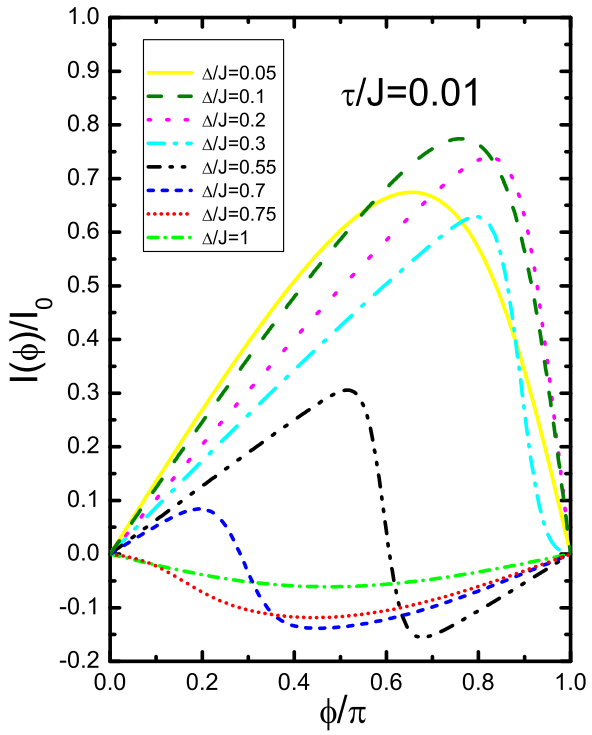

FIG. 5. (Color online) Josephson current $I(\varphi)/I_0$ as a function of φ, for $\tau/J = 0.01$ and different values of Δ/J.

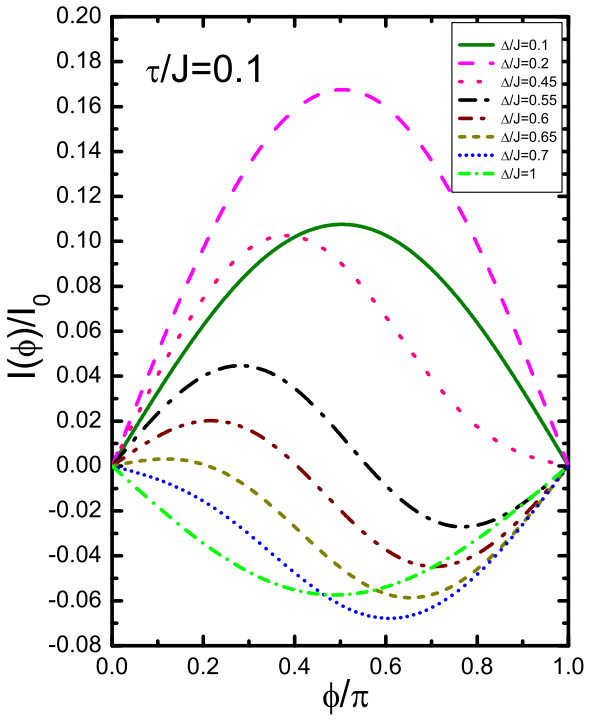

FIG. 6. (Color online) Josephson current $I(\varphi)/I_0$ as a function of φ, for $\tau/J = 0.1$ and different values of Δ/J. $I(\varphi)/I_0$ has a nonmonotonic behavior both in the regime of small and intermediate values of Δ/J.

Figure 6, which is the same as Fig. 5, but for $\tau/J = 0.10$, shows some important differences. In the first place, the amplitude of the Josephson current is about five times smaller as compared with the amplitudes in Fig. 5. Second, besides the nonmonotonic behavior in the regime of small Δ, the current also shows a second nonmonotonic behavior in the regime of intermediate Δ's. Clearly, for this temperature $I(\varphi)/I_0$ has a minimum in his amplitude for $0.55 \lesssim \Delta/J \lesssim 0.60$, increases for increasing Δ, and then decreases again for $\Delta/J = 1$. This somehow nontrivial behavior of the Josephson current with temperature and the strength of the unique parameter Δ/J is better displayed by looking at the critical current I_c/I_0.

Proceeding, in Fig. 7 we show the critical current I_c/I_0 as a function of Δ/J, for different values of temperature, in Fig. 8 we show the critical current as a function of τ/J, for different values of Δ/J, and in Fig. 9 we depict the "phase diagram" of the hybrid junction in Δ/J vs τ/J space. Starting with the analysis of Fig. 9, the full line shows the transition from the π' regime at lower T,Δ's to the π regime at higher T,Δ's. At zero temperature this transition occurs at $\Delta/J = 0.75$, as discussed above. The dashed line shows the transition from the $0'$ to the π' regime. It starts at zero temperature at $\Delta_c = J(1+\sqrt{17})/8 \simeq 0.64J$, and then decreases monotonically with temperature. The transition from the 0 to the $0'$ regime is indicated by the dotted line, and the case is that the 0-junction regime occurs only at finite temperatures. At $\tau \gtrsim 0.25$ and $\Delta/J \to 0$, all the curves collapse in one curve, where only one transition is possible from the 0 to the π regime. However, we must take into account that we neglected the temperature dependence of Δ and then we consider our results reliable only for $\Delta \gtrsim \tau$. The thin dashed straight line represents the limit $\Delta = \tau$, meaning that the part of the phase diagram below this line is not reliable. The thin full

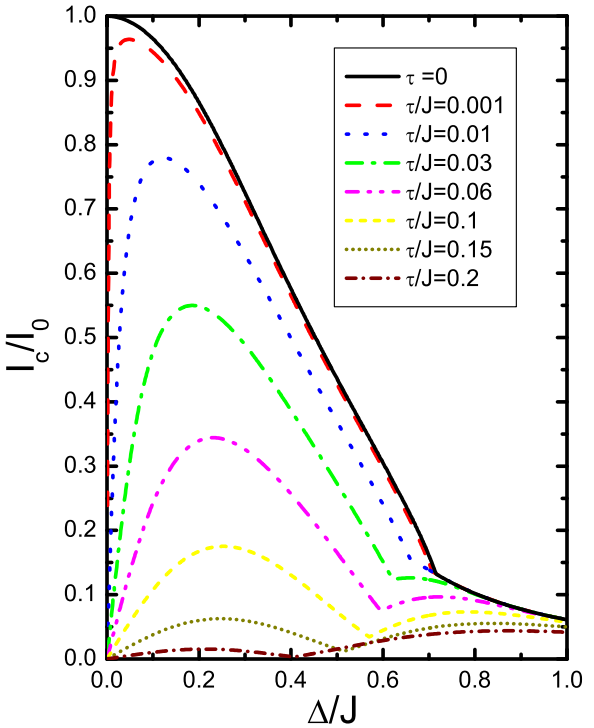

FIG. 7. (Color online) Critical current $I_c/I_0 = \max_\varphi |I(\varphi)|/I_0$ as a function of Δ/J for different values of τ/J. In all cases $I_c/I_0 \to 0$ for $\Delta \to 0$.

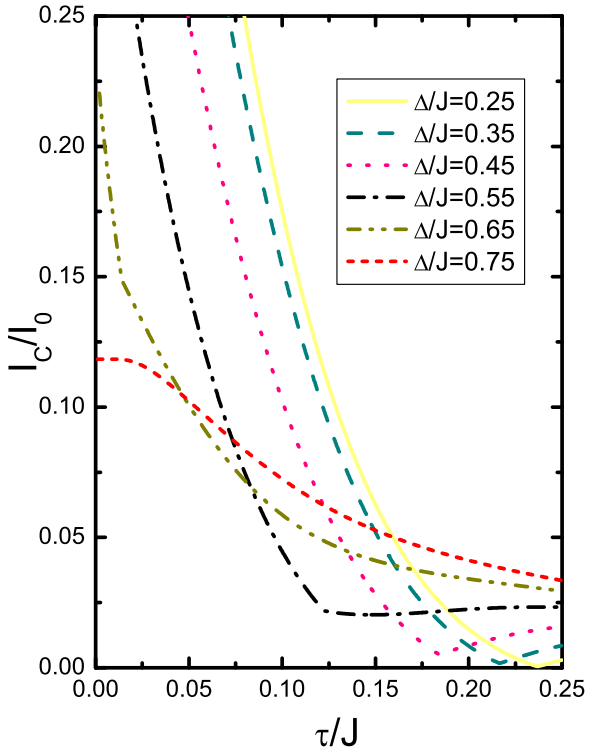

FIG. 8. (Color online) Critical current I_c/I_0 as a function of temperature, for several values of the superconducting order parameter. All curves have a finite value at $\tau = 0$, smaller than 1.

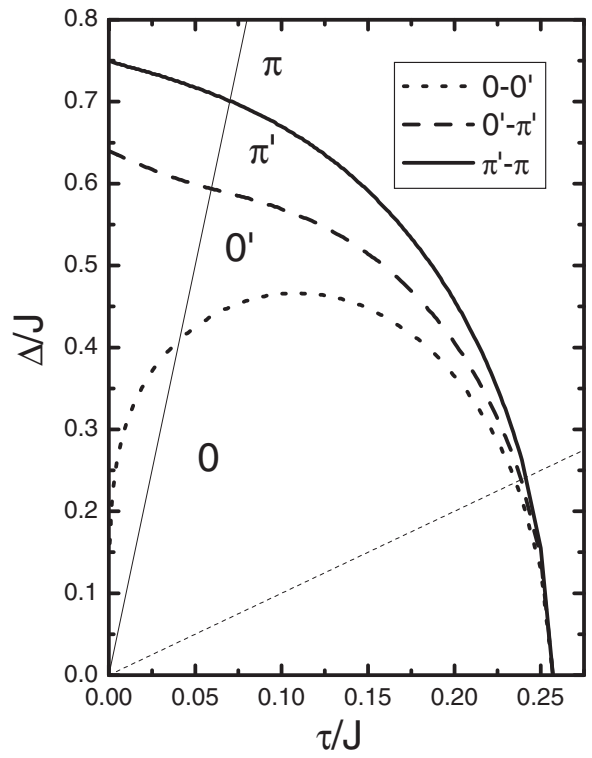

FIG. 9. Phase diagram in Δ/J, τ/J space. The analytical zero-temperature intercepts of the 0-0′, 0′-π', and π-π' boundaries are 0, $\Delta_c/J = (1+\sqrt{17})/8 \simeq 0.64$, and 0.75, respectively. The thin full straight line corresponds to $\Delta = 10\tau$, while the thin dashed straight line represents $\Delta = \tau$.

straight line corresponds to $\Delta = 10\tau$ and represents the line over which the authors in Ref. [20] perform the calculations. For the transitions, their results give $(\Delta/k_BT_K \sim 0.51)_{0-0'}$, $(\Delta/k_BT_K \sim 0.875)_{0'-\pi'}$, and $(\Delta/k_BT_K \sim 1.1)_{\pi'-\pi}$. Our results, in the Kondo limit ($U \to \infty$), are $(\Delta/J \sim 0.4)_{0-0'}$, $(\Delta/J \sim 0.6)_{0'-\pi'}$, and $(\Delta/J \sim 0.7)_{\pi'-\pi}$. In spite of the fact that the model parameters are not identical and the calculations are very different, our model results are in good quantitative agreement. The main message beyond the results in Fig. 9 is the fact that the Kondo-related 0- and 0′-junction configurations are dominant for $\Delta/J \lesssim 0.75$ and $\tau/J \lesssim 0.25$, and that by increasing Δ/J or/and τ/J the π'- and π-junction configurations become dominant. As we will see below, the fundamental 0′-π' boundary manifests clearly in the junction critical current, a fact that may be used for its experimental characterization.

Figure 7 displays then the behavior of the critical current as one moves vertically in the phase diagram, changing Δ/J at fixed τ. At zero temperature I_c/I_0 decreases monotonically with Δ/J. For $\Delta/J \lesssim 0.70$, I_c/I_0 is given by the maximum value of $I_0(\varphi)/I_0$. From Eq. (24) and considering that $I_0(\varphi)/I_0$ reaches its maximum value at $\varphi^*(\Delta/J)$ (see Fig. 3), we obtain that

$$\frac{I_c}{I_0} = \frac{I_0(\varphi^*)}{I_0} \tag{31}$$

in this Kondo-dominated regime. For $\Delta/J \gtrsim 0.70$, I_c/I_0 is given by the negative of the extreme value of $I_\pi(\varphi)/I_0$, which is (approximately) located at $\varphi/\pi = 1/2$. That is,

$$\frac{I_c}{I_0} \simeq -\frac{I_\pi(\pi/2)}{I_0} \tag{32}$$

in this superconductivity-dominated regime. According Eq. (28), for $\Delta/J \gg 1$, $I_c/I_0 \sim 3J^2/(64\Delta^2)$. The transition from one regime to the other is indicated by a change in slope for $\Delta/J \approx 0.70$. It is interesting to note that the change of regime from Eq. (31) to (32) occurs close (but not exactly) to the 0′ → π' transition in Fig. 9, slightly above the boundary, but clearly inside the π'-junction regime [44]. For $\tau \neq 0$, the current first increases (from zero) with Δ/J to reach a maximum at small values of Δ/J and then decreases when Δ/J is increased. This first maximum in the curve for I_c/I_0 vs Δ/J is then a natural consequence of the condition $I(\varphi = 0) = 0$ for $\Delta/J = 0$ at any τ [Eqs. (24) and (30)], and the fact that in the Kondo-dominated regime, the current must decrease for increasing Δ/J. Consistent with this, the Kondo-induced first maximum in I_c/I_0 decreases with increasing temperature showing the progressive loss of the Kondo correlations in the 0 and 0′ regimes. At very low temperatures, the critical current is essentially dominated by the singlet ground state (Kondo effect) of Eq. (15) that yields high values of I_c/I_0 close to the limiting value 1 ($\tau/J = 0.001, 0.01$). When τ is increased, the thermal excitations progressively destroy the Kondo correlations given an important reduction of the critical current ($\tau/J = 0.03$, 0.06, 0.1, 0.15, and 0.2). Simultaneously, the zero-temperature change of regime (slope discontinuity) around 0.7 evolves towards a local minimum for I_c/I_0 located close to the finite-temperature 0′ − π' boundary in Fig. 9 [20]. The appearance of this minimum has a straightforward explanation. Since the boundary between the 0′ and π'

regimes is defined by the condition that $\int_0^\pi d\varphi\, I(\varphi) = 0$, for this to be true, the amplitudes of the positive (Kondo-driven) and negative (superconductivity-driven) contributions to $I(\varphi)$ should be essentially the same, and relatively small (see, for example, the case $\Delta/J = 0.6$ in Fig. 6). Beyond this point, the negative component increases and the positive component decreases (see, for example, the cases $\Delta/J = 0.65, 0.7$ in Fig. 6), opening the way for the existence of a minimum for the critical current close to the boundary $0' - \pi'$. In brief, this minimum marks the change from a Kondo-dominated regime (for Δ's to the left of the minimum) to a superconductivity-dominated regime (for Δ's to the right of the minimum). The presence of a minimum in the curve I_c/I_0 vs Δ/J is also in good qualitative agreement with the QM results of Ref. [20], made on the single-temperature line $\tau = \Delta/10$. From their data, however, it is not possible to observe the first increase of I_c/I_0 for small values of Δ/J, presumably due to the fact that their first (smallest) value of Δ/T_K (the equivalent of Δ/J here) is already large [45]. Also, the existence of a local minimum was characterized by these authors as a "subtle many-body effect," for which we provide here a simple explanation, making the reasonable assumption that it is also valid for the full "standard" model. For increasing values of τ/J, the local minimum moves to smaller values of Δ/J, since the strength of the Kondo effect diminishes as the temperature rises. For large values of Δ/J, all critical current curves collapse to the one corresponding to the zero-temperature limit, which goes to zero as $(J/\Delta)^2$, as shown above. This is the reason for the existence of a second maximum beyond the local minimum. Interestingly, for $\tau/J \gtrsim 0.15$, the first maximum is smaller than the second one, and also we can see the crossings of curves ($\tau/J = 0.15$ and $\tau/J = 0.2$) at $\Delta/J \sim 0.5$. This suggests the existence of an "anomalous" regime at small values of the critical current, such that when τ is increased, I_c/I_0 is also increased.

We display such anomalous behavior in Fig. 8, using for now the critical current I_c/I_0 as a function of τ/J, for different values of Δ/J. For $\Delta/J \geqslant 0.75$, at any value of temperature the junction is π type (see Fig. 9), and I_c/I_0 decreases monotonically with τ/J ($\Delta/J = 0.75$). For $\Delta/J = 0.65$ we can observe, at low temperatures, a different behavior of I_c/I_0, with a change in slope around the transition between $0'$ and π' regimes. For $\Delta/J = 0.55$ the curve shows how the change in slope at $\tau/J \sim 0.125$ evolves towards a smooth local minimum. Similar behavior is obtained for $\Delta/J = 0.45$, $\Delta/J = 0.35$, and $\Delta/J = 0.25$, where we can see a well defined minimum for $\tau/J \sim 0.18$, $\tau/J \sim 0.21$, and $\tau/J \sim 0.23$, respectively. For higher values of τ/J beyond this minimum, I_c/I_0 shows the anomalous behavior commented on above, increasing with increasing temperature. This kind of behavior has been observed experimentally in Ref. [17], where the coupling of two superconductors through a ferromagnet link was studied. As in the previous case of Fig. 7, these minima in Fig. 8 mark the transition from a Kondo dominated regime at low temperatures to a superconductivity dominated regime at higher temperatures. As before, the minima are located slightly above the $0' - \pi'$ boundary in Fig. 9.

IV. CONCLUSIONS

We have applied the narrow-band approximation to analyze the Josephson current through a quantum dot connected between superconducting electrodes, when the dot is in the Kondo limit. The model is completely characterized by the dimensionless parameter Δ/J, with Δ the superconducting order parameter, and J the antiferromagnetic Kondo exchange strength. Each of the two narrow-band superconducting banks can be occupied by zero, one, or two electrons at most, and this simplifies drastically the calculations, without losing any of the main physical ingredients of the full standard model. As a proof of that, we have reproduced all the known zero- and finite-temperature features of the full model, as follows: (i) qualitative agreement between the first and second many-body excited states of the full model and the lowest-lying eigenvalues of the present narrow-band model; (ii) four types of hybrid junction configurations (0, $0'$, π', π); (iii) a nonmonotonic behavior of the junction critical current, at fixed temperature and for increasing values of Δ/J. The simplicity of the model allows us to provide a transparent physical explanation for each of these features, something that is not always possible with the much more involved calculations needed for the full model.

We also provide evidence for a nonmonotonic behavior of the critical current for increasing temperatures, at fixed values of Δ/J, and just before the junction enters in the π-junction regime. This finding should be possible to be checked experimentally. And, finally, we summarize our findings in a global phase diagram in the space Δ/J, k_BT/J, showing the evolution and stability of the four possible junction configurations with superconductivity strength and temperature. This global phase diagram should be useful for further experimental and theoretical developments alike, by providing an overall picture of the hybrid junction system.

ACKNOWLEDGMENTS

The authors acknowledge many useful discussions with Blas Alascio. R.J.A. was supported by the Consejo Nacional de Investigaciones Científicas y Técnicas (CONICET). C.R.P. thanks CONICET for partial financial support and ANPCyT under Grant No. PICT-2012-0379.

[1] S. D. Franceschi, L. Kouwenhoven, C. Schönenberger, and W. Wernsdorfer, Nat. Nanotechnol. **5**, 703 (2010).

[2] D. Goldhaber-Gordon, H. Shtrikman, D. Mahalu, D. Abusch-Magder, U. Meirav, and M. A. Kastner, Nature (London) **391**, 156 (1998).

[3] S. J. Tans, M. H. Devoret, H. Dai, A. Thess, R. E. Smalley, L. J. Geerligs, and C. Dekker, Nature (London) **386**, 474 (1997).

[4] J. Nygard, D. H. Cobden, and P. E. Lindelof, Nature (London) **408**, 342 (2000).

[5] J. Park, A. N. Pasupathy, J. I. Goldsmith, C. Chang, Y. Yaish, J. R. Petta, M. Rinkoski, J. P. Sethna, H. D. Abrua, P. L. McEuen, and D. C. Ralph, Nature (London) **417**, 722 (2002).

[6] L. P. Kouwenhoven, C. M. Marcus, P. L. McEuen, S. Tarucha, R. M. Westervelt, and N. S. Wingreen, in *Mesoscopic Electron Transport*, edited by L. L. Sohn, L. P. Kouwenhoven, and G. Schön (Kluwer, Dordrecht, The Netherlands, 1997).

[7] P. G. de Gennes, *Superconductivity of Metals and Alloys* (Addison-Wesley, Redwood City, CA, 1966).

[8] R. C. Jaklevic, J. Lambe, A. H. Silver, and J. E. Mercereau, Phys. Rev. Lett. **12**, 159 (1964).

[9] J. Clarke and F. K. Wilhelm, Nature (London) **453**, 1031 (2008).

[10] I. N. Bulaevskii, V. V. Kuzii, and A. A. Sobyanin, JETP Letters **25**, 290 (1977).

[11] E. A. Jagla and C. A. Balseiro, Solid State Commun. **93**, 119 (1995).

[12] K. K. Likharev, Rev. Mod. Phys. **51**, 101 (1979).

[13] R. Maurand, T. Meng, E. Bonet, S. Florens, L. Marty, and W. Wernsdorfer, Phys. Rev. X **2**, 011009 (2012).

[14] B.-K. Kim, Y.-H. Ahn, J.-J. Kim, M.-S. Choi, M.-H. Bae, K. Kang, J. S. Lim, R. López, and N. Kim, Phys. Rev. Lett. **110**, 076803 (2013).

[15] E. J. H. Lee, X. Jiang, M. Houzet, R. Aguado, C. M. Lieber, and S. De Franceschi, Nat. Nanotechnol. **9**, 79 (2013).

[16] J.-D. Pillet, P. Joyez, R. Žitko, and M. F. Goffman, Phys. Rev. B **88**, 045101 (2013).

[17] V. V. Ryazanov, V. A. Oboznov, A. Yu. Rusanov, A. V. Veretennikov, A. A. Golubov, and J. Aarts, Phys. Rev. Lett. **86**, 2427 (2001).

[18] V. Mourik, K. Zuo, S. M. Frolov, S. R. Plissard, E. P. A. M. Blakkers, and L. P. Kouwenhoven, Science **336**, 1003 (2012).

[19] A. Martín-Rodero and A. Levy Yeyati, Adv. Phys. **60**, 899 (2011).

[20] F. Siano and R. Egger, Phys. Rev. Lett. **93**, 047002 (2004); **94**, 039902(E) (2005).

[21] M.-S. Choi, M. Lee, K. Kang, and W. Belzig, Phys. Rev. B **70**, 020502 (2004).

[22] C. Karrasch, A. Oguri, and V. Meden, Phys. Rev. B **77**, 024517 (2008).

[23] A. A. Clerk and V. Ambegaokar, Phys. Rev. B **61**, 9109 (2000).

[24] G. Sellier, T. Kopp, J. Kroha, and Y. S. Barash, Phys. Rev. B **72**, 174502 (2005).

[25] T. Meng, S. Florens, and P. Simon, Phys. Rev. B **79**, 224521 (2009).

[26] D. J. Luitz, F. F. Assaad, T. Novotny, C. Karrasch, and V. Meden, Phys. Rev. Lett. **108**, 227001 (2012).

[27] T. Domański, J. Barański, and Z. Zapalska, Philos. Mag. (2014), doi: 10.1080/14786435.2014.965766.

[28] R. Allub and C. R. Proetto, Phys. Rev. B **62**, 10923 (2000); Solid State Commun. **117**, 429 (2001).

[29] E. Vecino, A. Martín-Rodero, and A. Levy Yeyati, Phys. Rev. B **68**, 035105 (2003).

[30] F. S. Bergeret, A. Levy Yeyati, and A. Martín-Rodero, Phys. Rev. B **76**, 174510 (2007).

[31] I. Affleck, J.-S. Caux, and A. M. Zagoskin, Phys. Rev. B **62**, 1433 (2000).

[32] J. R. Schrieffer and P. A. Wolff, Phys. Rev. **149**, 491 (1966).

[33] C. R. Proetto and A. López, Solid State Commun. **37**, 745 (1981); Phys. Rev. B **24**, 3031 (1981).

[34] B. Alascio, R. Allub, and A. Aligia, J. Phys. C **13**, 2869 (1980).

[35] A. N. Kocharyan, P. S. Ovnanyan, and D. I. Khomskii, JETP Letters **34**, 23 (1981).

[36] E. Artacho and L. M. Falicov, Phys. Rev. B **47**, 1190 (1993).

[37] R. Allub, C. Wiecko, and B. Alascio, Phys. Rev. B **23**, 1122 (1981).

[38] R. Allub, M. Achterberg, and B. Alascio, Phys. Rev. B **30**, 5349 (1984).

[39] R. Allub, Phys. Rev. B **67**, 144416 (2003); J. Phys.: Condens. Matter **20**, 445204 (2008).

[40] P. Fulde, *Electron Correlations in Molecules and Solids* (Springer, New York, 1995), p. 284.

[41] A. C. Hewson, *The Kondo Problem to Heavy Fermions* (Cambridge University Press, Cambridge, UK, 1993), p. 371.

[42] G. Gross and G. P. Parravicini, *Solid State Physics* (Academic Press, New York, 2000), p. 608.

[43] J. E. Hirsch and R. M. Fye, Phys. Rev. Lett. **56**, 2521 (1986).

[44] This is easily seen from Fig. 3, from the fact that $I_0(\varphi^*)/I_0 > -I_\pi(\pi/2)/I_0$ for $\Delta = \Delta_c \simeq 0.64J$.

[45] The following argument provides an estimate of the Kondo temperature $T_K^{\rm NB}$ for the present narrow-band (NB) system. The eigenvalues of $\tilde{H}_K$ of Eq. (10) are $-3J/4$ (ground-state, singlet) and $J/4$ (triplet). Assuming that the free energy of the singlet and triplet configurations becomes the same at $T_K^{\rm NB}$, we have that $-3J/4 = J/4 - k_B T \ln(3)$. Solving, we obtain $k_B T_K^{\rm NB} = J/\ln(3) \simeq 0.91J$. This linear dependence of $T_K^{\rm NB}$ with J is the main drawback of the NB approximation; it is well known that the Kondo temperature of the full system has an exponential dependence on J. This prevents us from making quantitative predictions for real systems. However, as shown above, once the reasonable identification $J \sim T_K^{\rm NB} \to T_K$ is made, all the thermodynamics of the model is in qualitative agreement with available finite-temperature results for the full system.